Paramagnetic Organometallic Molecules. 9.[1] Metal-Metal Interaction in $X_2Co_2(CO)_6$. Analysis of the ESR Spectra of $[RC_2R']Co_2(CO)_6^-\cdot$

Barrie M. Peake,[2a] Philip H. Rieger,*[2b] Brian H. Robinson,[2a] and Jim Simpson[2a]

Contribution from the Departments of Chemistry, Brown University, Providence, Rhode Island 02912, and University of Otago, Box 56, Dunedin, New Zealand. *Received July 2, 1979*

Abstract: The ESR spectra of electrolytically generated anion radicals of several acetylene-bridged dicobalt hexacarbonyls, $RC_2R'Co_2(CO)_6^-\cdot$, were observed in THF solutions. The isotropic spectra show coupling to two equivalent cobalt nuclei with $\langle a \rangle$ = 2.4–2.8 mT and $\langle g \rangle$ = 2.010–2.015. Frozen solution ESR spectra were interpreted in terms of completely anisotropic g and cobalt hyperfine tensors. One of the hyperfine tensor principal axes is parallel to the corresponding g-tensor axis, but the other two hyperfine tensor axes are oriented at ±15–20° relative to the g-tensor axes. This information and the magnitude of the hyperfine tensor components allow the following conclusions to be drawn: (1) the unpaired electron occupies a b_2 orbital, largely cobalt $3d_{z^2}$ in character, with the major axes of the metal 3d contributions oriented at 15–20° relative to the Co–Co vector; (2) the total cobalt 3d contribution to the orbital is about 64%; (3) the isotropic coupling is negative, implying a total cobalt 4s contribution of about 1.6%; (4) to the extent that the unpaired electron occupies the antibonding counterpart of the a_1 metal–metal bonding orbital, the Co–Co bond may be accurately described as a "bent" bond.

Introduction

When one considers ESR spectra of polynuclear organometallic radicals which have a single unpaired electron delocalized over two or more metal atoms, one naturally thinks of analogies with polynuclear complexes of paramagnetic transition metal ions (e.g., dimeric oxovanadium(IV)[3] or copper(II)[4] tartrates) or with organic π radicals. The situation is quite different than for either of these apparent analogues, however. Electron delocalization reduces spin–orbit coupling so that g-tensor anisotropy is small and, with only one unpaired electron, there are no complicating spin exchange effects or zero-field splittings. Thus these species afford much simpler ESR spectra than typical polynuclear complexes. On the other hand, unlike π radicals, isotropic nuclear hyperfine couplings can, by themselves, give relatively little information. The isotropic cobalt coupling in an organocobalt radical, for example, arises[5] from polarization of the filled 1s and 2s orbitals, giving negative contributions to $\langle a^{Co} \rangle$, from polarization of the 3s orbital and filled molecular orbitals with 4s character, giving positive contributions to $\langle a^{Co} \rangle$, and from admixture of 4s character into the molecular orbital containing the unpaired electron, again giving a positive contribution to $\langle a^{Co} \rangle$. The observed isotropic cobalt coupling is thus a balance among these five contributions, and, although some trends in a series of related radicals may be understandable, it is unlikely that an observed coupling constant can, by itself, yield much useful information about the spin density distribution in the molecule.

It has long been recognized[6] that the electron–nuclear hyperfine interaction tensor, obtained from ESR spectra of paramagnetic species in dilute single crystals, has both magnitude and directional information and that this information can be used to construct a rather detailed description of the orbital containing the unpaired electron. It is usually assumed that ESR powder patterns, lacking a reference direction, can yield only the magnitudes of the hyperfine tensor components. Though this is often true, some directional information is retained in the ESR powder patterns of radicals containing two or more equivalent magnetic nuclei. As we shall demonstrate, the experimental spectrum is sensitive to the relative orientations of the principal axes of the various hyperfine tensors, and furthermore these orientations can be obtained, at least approximately, from experimental spectra.

In this paper, we report the interpretation of frozen solution ESR spectra of a series of acetylene-bridged dinuclear cobalt radical anions, $RC_2R'Co_2(CO)_6^-\cdot$,[7] to obtain the cobalt hyperfine tensors and the relative orientations of the tensor principal axes. This information will be used to construct a detailed description of the molecular orbital containing the unpaired electron. It is generally accepted that a distinct cobalt–cobalt bond is required to rationalize the geometry and diamagnetism of the parent molecules, but there has been some difference of opinion as to whether it is a "straight" or "bent" interaction.[8] Results for molecular-orbital calculations[9,10] on $X_2M_2(CO)_6$ systems favor the "bent" bond model and this is unequivocally demonstrated in this paper.

Frozen Solution ESR Spectra

In this section, we will discuss the general expectations for ESR spectra of frozen solutions of paramagnetic molecules containing two or more magnetic nuclei with anisotropic hyperfine coupling tensors. We shall assume one unpaired electron, small g-tensor anisotropy, and negligible quadrupolar coupling.

The ESR spectrum of a sample of randomly oriented paramagnetic molecules, each with n magnetic nuclei, consists of the superposition of $(2I_1 + 1)\ldots(2I_n + 1)$ components, corresponding to all possible combinations of nuclear spin quantum numbers. For one component, magnetic resonance absorption occurs at a magnetic field given to first order by

$$B = B_0 - \sum_i m_i k_i \qquad (1)$$

where $B_0 = h\nu_0/g\mu_B$ and m_i is the nuclear spin quantum number of the ith nucleus; g and k_i, the effective g value and the ith nuclear hyperfine coupling constant, are functions of the g and hyperfine tensor components, g_v and a_{iv}, and of the angles θ and ϕ which describe the orientation of **B** in the coordinate system defined by the principal axes of the g tensor. For a randomly oriented sample, absorption occurs over a field range determined by the range of g and the k_i when θ ranges from 0 to 180° and ϕ ranges from 0 to 360°.

Component powder patterns computed using eq 1 generally have the shape shown in Figure 1a. A variety of homogeneous and inhomogeneous broadening mechanisms round off the discontinuities on the absorption powder pattern as shown in

0002-7863/80/1502-0156$01.00/0

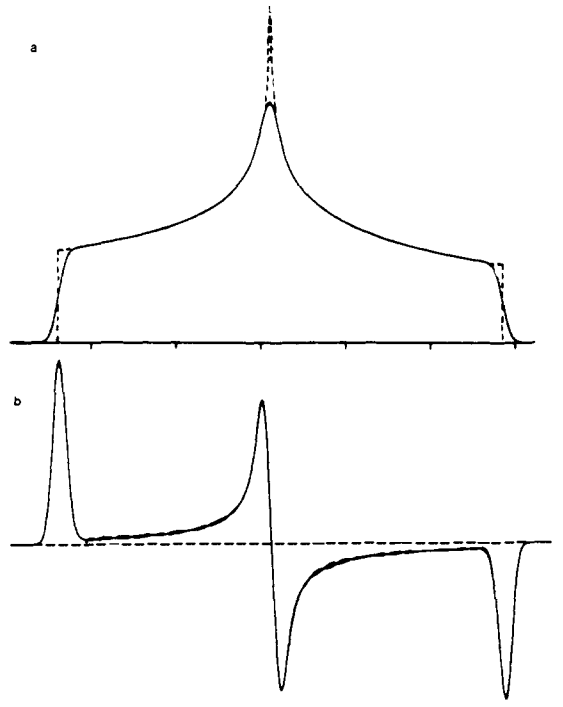

Figure 1. Component powder pattern: (a) absorption (dashed lines show unbroadened absorption line shape); (b) first derivative of absorption.

the figure so that the first derivative powder pattern shown in Figure 1b is obtained. The complete spectrum then is a superposition of these component powder patterns.

When the first-order result, eq 1, suffices (i.e., when the high-field approximation is valid, $|a_{iv}/B| \ll 1$), and when the principal axes of the hyperfine tensors and g tensor are coincident, the recognizable features of the derivative spectrum may be grouped into three series of features, each described by eq 1, where the g and k_i are, successively, the three elements of the diagonal g and hyperfine tensors. In other words, three series of features are found, the spacing and centers of gravity of which may be measured to determine g_1 and the a_{i1}, g_2 and the a_{i2}, and g_3 and the a_{i3}.

Complications may arise in the interpretation of frozen solution spectra when one or more of the a_{iv} is sufficiently large that the high-field approximation breaks down. The introduction of second-order terms in the solution of the spin Hamiltonian leads to a corrected form of eq 1 for the positions of the derivative spectrum features:[11]

$$B_v = B_0 - \sum_i a_{iv}m_i - \sum_i \left[\frac{I_i(I_i+1) - m_i^2}{4B_0}\right] \times \left[\left(\frac{g_t}{g_v}\right)^2 a_{it}^2 + \left(\frac{g_u}{g_v}\right)^2 a_{iu}^2\right] \quad (2)$$

where $B_0 = h\nu_0/g_v\mu_B$ and the indices t, u, and v refer to the three principal axes of the tensors. The second-order term in eq 2 leads to variations in the spacings of spectral features and shifts the center of gravity downfield from B_0; corrections must in general be made to obtain accurate values of the g and a_i tensor components.

In contrast to an isotropic solution where reorientation correlation times are very short and symmetrically equivalent nuclei are magnetically equivalent over an interval of time defined by the line widths, symmetrically equivalent nuclei in a frozen solution are magnetically inequivalent for many orientations. For this reason, eq 2 was derived using the uncoupled representation with $|m_S, m_1, m_2, \ldots\rangle$ as basis functions. In principle, the coupled representation with basis functions m_S, J, M should be used for those orientations in which symmetrically equivalent nuclei are also magnetically equivalent.[12] In the coupled representation, the second-order term of eq 2 is replaced by

$$-\left[\frac{J(J+1) - M^2}{4B_0}\right]\left[\left(\frac{g_t}{g_v}\right)^2 a_t^2 + \left(\frac{g_u}{g_v}\right)^2 a_u^2\right] \quad (3)$$

The second-order corrections of eq 3 may be much larger or much smaller than those of eq 2, depending on the value of J. Thus, when one or more of the tensor components is large, extra features, corresponding to those angles for which the nuclei are magnetically equivalent, may be observed in the spectrum. This effect is most often lost within the line widths, however, and, since the *average* second-order shifts of components within a "line" corresponding to a given value of $M = \Sigma m_i$ is the same in the two representations, these complications are not generally expected.

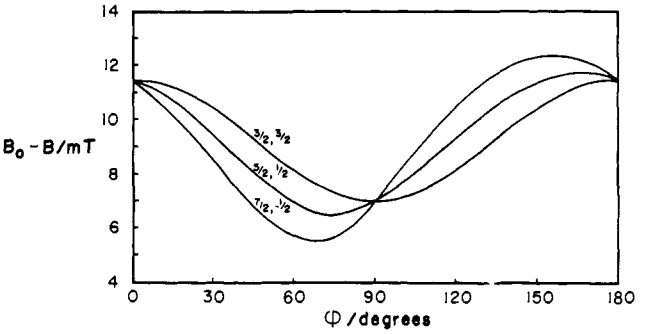

Figure 2. Resonant field as a function of orientation in the $\theta = 90°$ plane for $m_1 + m_2 = 3$, $a_2 = 4$ mT, $a_3 = 2$ mT, $\alpha = \pm 20°$.

When the principal axes of the g and hyperfine tensors are parallel, the observed spectral features correspond to orientations where the magnetic field is aligned with one of the principal axes, i.e., to $\theta = 0$, to $\theta = 90°$, $\phi = 0°$, or to $\theta = 90°$, $\phi = 90°$. When the principal axes are not parallel, however, the observed features do not necessarily correspond with orientations along the g tensor principal axes and spacings of features in general are functions of two (or three) of the hyperfine tensor components.

Consider, for example, the case of two symmetrically equivalent nuclei where one of the principal axes for each hyperfine tensor is coincident with a g-tensor axis; the other two hyperfine tensor axes are rotated by an angle α from the corresponding g-tensor axes for one nucleus and by $-\alpha$ for the other nucleus. Then, neglecting g-tensor anisotropy, the resonant field is given to first order by eq 4. Thus one series of features, corresponding to $\theta = 0$, is expected at $B = B_0 - a_1(m_1 + m_2)$. The other features correspond to $\theta = 90°$ and the values of ϕ which maximize and minimize $m_1b_+ + m_2b_-$. Consider, for example, the $M = 3$ components when $a_2 = 4$ mT, $a_3 = 2$ mT, and $\alpha = 20°$. The quantity $B_0 - B$ is plotted as a function of the angle ϕ in Figure 2. Maxima occur at $B_0 - B = 12.4$, 11.7, and 11.4 mT for the ($^7/_2$, $-$ $^1/_2$), ($^5/_2$, $^1/_2$), and ($^3/_2$, $^3/_2$) components, respectively, while minima are at $B_0 - B = 5.5$, 6.5, and 7.0 mT for the same components. If the hyperfine tensor axes were coincident, the extrema would have occurred at $B_0 - B = 12.0$ and 6.0 mT for all components. Thus substantial shifts and splittings are expected when the tensor axes are not collinear. In practice, the components may not be resolved, but the width of observed features should increase with decreasing $|M|$ and averaged features should not be equally spaced, even after correcting for second-order shifts.

$$B = B_0 - m_1k_+ - m_2k_- \quad (4)$$

$$k_\pm = (a_1^2\cos^2\theta + b_\pm^2\sin^2\theta)^{1/2} \quad (5)$$

$$b_\pm = [a_2^2\cos^2(\phi \pm \alpha) + a_3^2\sin^2(\phi \pm \alpha)]^{1/2} \quad (6)$$

Table I. Isotropic ESR Parameters

radical anion	$\langle g \rangle^a$	$\langle a \rangle$/mT	t_{max}/°C[b]
$[C_6H_5C_2Si(CH_3)_3]Co_2(CO)_6^-\cdot$ (**1**)	2.011	−2.88 ± 0.01	−60
$[CH_3C_2Si(CH_3)_3]Co_2(CO)_6^-\cdot$ (**2**)	2.012	−2.86 ± 0.02	−60
$[(C_6H_5)_2C_2]Co_2(CO)_6^-\cdot$ (**3**)	2.010	−2.84 ± 0.04	−60
$[(t\text{-}C_4H_9)_2C_2]Co_2(CO)_6^-\cdot$ (**4**)	2.009	−2.84 ± 0.02	−50
$[H_2C_2]Co_2(CO)_6^-\cdot$ (**5**)	2.010	−2.63 ± 0.02	−70
$[CF_3C_2Si(CH_3)_3]Co_2(CO)_6^-\cdot$ (**6**)	2.013	−2.66 ± 0.01	0
$[(CF_3)_2C_2]Co_2(CO)_6^-\cdot$ (**7**)	2.015	−2.37 ± 0.01	+20
$P_2Co_2(CO)_6^-\cdot$ (**8**)	2.007	−2.80 ± 0.03[c]	+20
$As_2Co_2(CO)_6^-\cdot$ (**9**)	2.012	−2.81 ± 0.01[d]	0

[a] Estimated uncertainty ±0.001. [b] Temperature at which radical lifetime is about 1 min in THF. [c] $|\langle a^P \rangle| = 3.74 \pm 0.06$ mT. [d] $|\langle a^{As} \rangle| = 2.12 \pm 0.05$ mT.

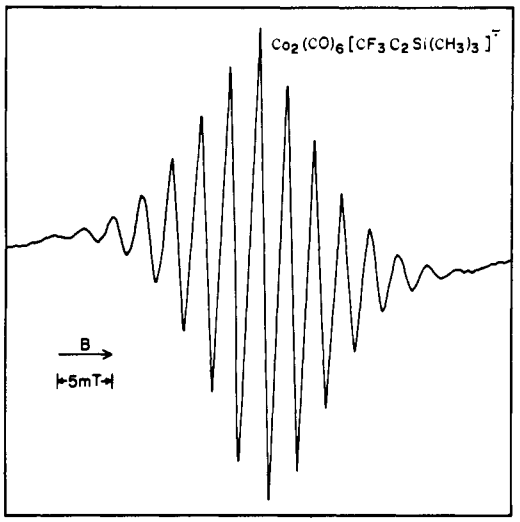

Figure 3. ESR spectrum of $[CF_3C_2Si(CH_3)_3]Co_2(CO)_6^-\cdot$ in THF solution at −50 °C.

Experimental Section

ESR spectra were obtained with a Varian E-4 spectrometer equipped with a variable temperature accessory. The microwave frequency was determined with a Systron-Donner microwave frequency counter and the Fieldial calibration was checked by proton resonance. The acetylene-bridged dicobalt compounds were synthesized by literature methods[13] or were supplied by Dr. R. J. Dickson. Tetrahydrofuran solvent was distilled from benzophenone ketyl and tetra-*n*-butylammonium perchlorate was used as the supporting electrolyte. Radical anions were produced by electrolysis in situ in the ESR cavity, usually at −60 °C; frozen solution spectra were obtained by cooling the resulting solution to −160 °C.

Results

Isotropic Spectra. ESR spectra of liquid THF solutions of the $RC_2R'Co_2(CO)_6$ radical anions show the expected 15 hyperfine lines due to interaction of the unpaired electron with two equivalent spin 7/2 cobalt-59 nuclei. A typical spectrum, that of $[CF_3C_2Si(CH_3)_3]Co_2(CO)_6^-\cdot$ obtained at −50 °C, is shown in Figure 3. Isotropic g values and cobalt hyperfine coupling constants are given in Table I. Spectra were obtained from −70 °C up to the maximum temperatures given in Table I; the isotropic g values and cobalt hyperfine coupling constants are independent of temperature within the error limits given in the table.

Frozen Solution Spectra. Reduction of the temperature of a THF solution of a $RC_2R'Co_2(CO)_6$ radical anion, produced at −60 °C, to −160 °C resulted in ESR spectra similar in all cases to that of $[CF_3C_2Si(CH_3)_3]Co_2(CO)_6^-\cdot$ which is shown in Figure 4. The spectrum of this particular radical was slightly better resolved than the others and was therefore chosen for

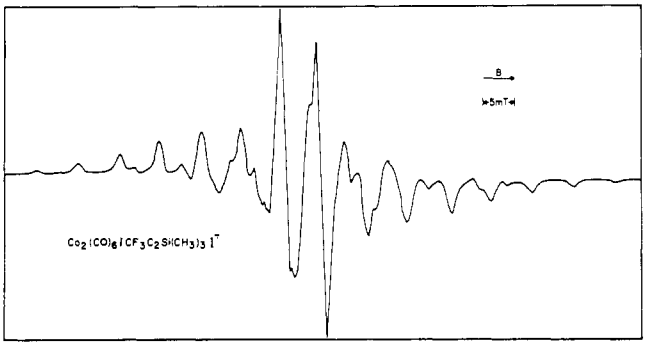

Figure 4. ESR spectrum of $[CF_3C_2Si(CH_3)_3]Co_2(CO)_6^-\cdot$ in THF solution at −160 °C.

detailed analysis and interpretation. The spectrum was analyzed in two stages: first by assignment of the more prominent features, direct measurement of positions, and least-squares fitting to eq 2; second by computer simulation of the spectrum and refinement by "cut and try" methods to obtain the parameters not uniquely determined by visual observation.

Examination of the frozen solution spectrum, Figure 4, clearly reveals a series of prominent, nearly equally spaced features, approximately equal in width, which increase in amplitude from the wings of the spectrum toward the center. These features clearly correspond to the largest hyperfine tensor component. Since there is no evidence of additional splitting of these components, unusual line shapes, broadening, or marked deviation from the expected intensity ratios, they must correspond to a hyperfine tensor principal axis which is collinear with one of the g-tensor axes. From the positions of these components, g_1 and a_1 were determined by least-squares fit to eq 2, at first to first order, and, later when estimates of a_2 and a_3 were available, to second order. The final result is $g_1 = 2.007$, $|a_1| = 6.49 \pm 0.02$ mT.

After assignment of the features corresponding to a_1, several well-resolved features remain in the wings of the spectrum which have shapes analogous to the central feature of the component powder pattern shown in Figure 1b. It is easy to show that these correspond to a second tensor component with $M = -7, -5, +4, +6$, and $+7$ (assuming $a_2 < 0$), and that, with this assignment, other expected features in the series would be obscured by overlap with the more prominent a_1 features. Other assignments lead to predictions of components in regions where no feature is observed. These features are not exactly equally spaced (even after correction for second-order shifts and approximate overlap corrections), vary somewhat in width and shape, and do not increase in amplitude with decreasing $|M|$ as rapidly as do the a_1 features. For these reasons, it is likely that these features are due to a tensor component corresponding to principal axes not coincident with g-tensor axes. Nonetheless, it is possible to determine $g_2 = 2.012$ and estimate $|a_2| \simeq 4.2$ mT. From this and the requirement that

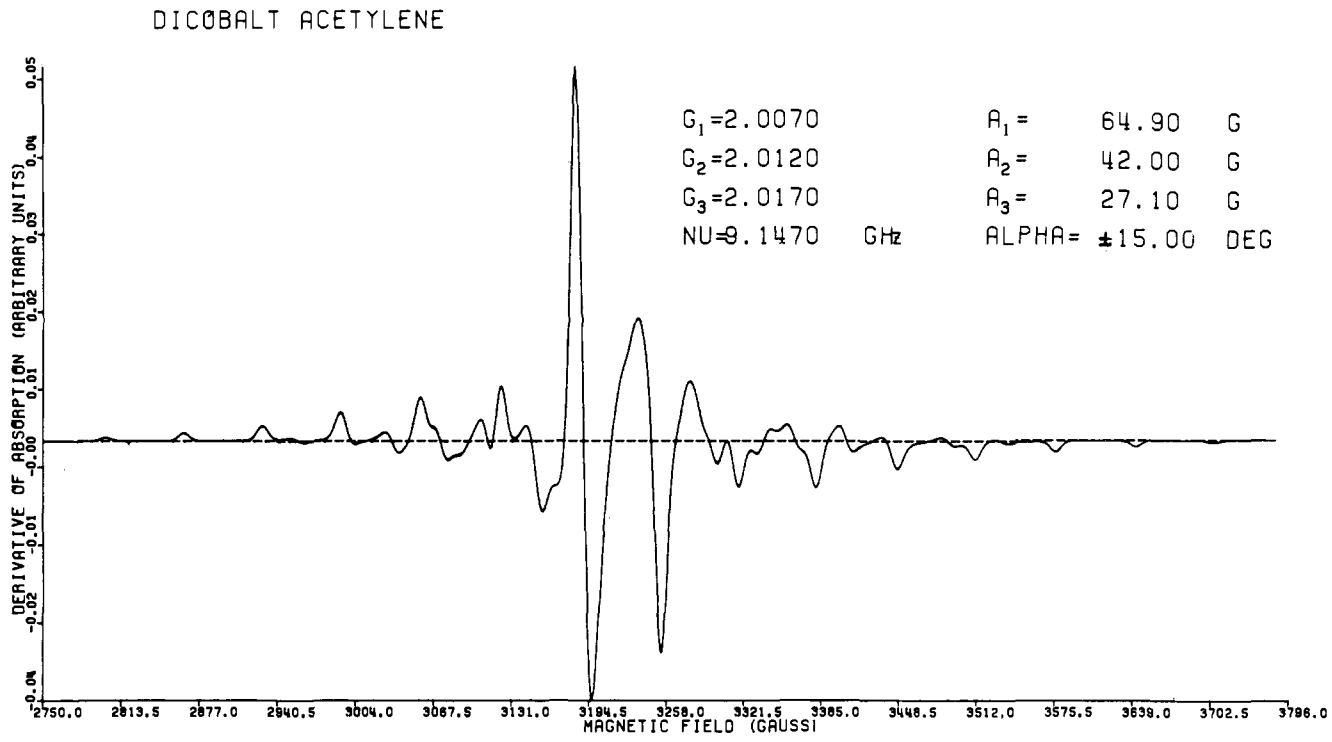

Figure 5. Computer-simulated spectrum of $[CF_3C_2Si(CH_3)_3]Co_2(CO)_6^{-\bullet}$ for $\alpha = \pm 15°$ and the parameters given in Table II.

Table II. Anisotropic ESR Parameters

radical	g_1[a]	g_2[a]	g_3[b]	a_1/mT	a_2/mT	a_3/mT
1	2.002	[c]	[c]	−6.69 ± 0.02	[c]	[c]
2	2.005	2.011	2.020	−6.68 ± 0.01	−4.44 ± 0.03	2.54 ± 0.05
3	2.000	2.011	2.019	−6.62 ± 0.02	−4.15 ± 0.03	2.25 ± 0.08
4	1.998	2.020	2.009	−6.75 ± 0.01	−3.83 ± 0.02	2.06 ± 0.04
5	2.002	[c]	[c]	−6.60 ± 0.03	[c]	[c]
6	2.007	2.012	2.017	−6.49 ± 0.01	−4.20 ± 0.02	2.71 ± 0.03
7	2.009	2.013	2.024	−6.22 ± 0.02	−3.89 ± 0.03	3.00 ± 0.04

[a] Estimated uncertainty ±0.002. [b] Estimated uncertainty ±0.005. [c] Frozen solution spectrum features unresolved.

the isotropic $\langle g \rangle$ and $\langle a \rangle$ are given by

$$\langle g \rangle = (g_1 + g_2 + g_3)/3 \quad (7)$$

$$\langle a \rangle = (a_1 + a_2 + a_3)/3 \quad (8)$$

we can estimate $g_3 \simeq 2.02$, $|a_3| \simeq 2.7$ mT. It is necessary that $\langle a \rangle$, a_1, and a_2 all have the same sign and that a_3 be of opposite sign in order to avoid the prediction of unobserved features. A number of partially resolved features in the experimental spectrum may be assigned tentatively to the a_3 features, but direct interpretation can go little further than the results quoted.

In further analysis of the spectrum, it was assumed that the two cobalt nuclei are symmetrically equivalent as indicated by the isotropic spectrum and that the hyperfine tensor principal axes for each cobalt corresponding to a_1 are coincident with the g_1 principal axis. The other two pairs of hyperfine tensor axes are then assumed to be symmetrically displaced from the g-tensor axes, i.e., $\alpha_1 = -\alpha_2$. Since the $M = \pm 7$ features of the a_2 series are well resolved and must correspond to $\theta = 90°$, $\phi = 0°$, a useful constraint on parameter choices is provided by the separation of these two features:

$$B(+7) - B(-7) = [a_2^2 \cos^2 \alpha + (g_3/g_2)^2 a_3^2 \sin^2 \alpha]^{1/2} \quad (9)$$

Two other constraints are provided by eq 7 and 8. Thus of the seven parameters—g_1, g_2, g_3, a_1, a_2, a_3, and α—three are accurately known and three reasonably accurate constraints are available, leaving one degree of freedom.

The spectrum was then computer simulated, using the program described in the Appendix, for $0° \leq \alpha \leq 30°$, varying a_2 and a_3 in accord with the constraints, eq 8 and 9; the value of g_3 was also varied within the range permitted by the experimental uncertainty in eq 7. The simulations were found to be generally rather insensitive to the value of a_3 for $\alpha > 10°$, but were quite sensitive to α. This is as expected since the broadening resulting from noncoincident tensor axes is greatest for the features due to the smallest component (see Figure 2). In all, 25 simulations were produced with the best fits obtained when α was 15–20°. The simulation for $\alpha = 15°$ is shown in Figure 5 and the corresponding parameters are listed in Table II. Although the fit is almost certainly optimum for the spin Hamiltonian assumed, eq A1, it is not perfect. A completely satisfactory fit would probably require the inclusion of nuclear quadrupole coupling. Belford and Duan[14] have shown that the "forbidden" transitions which arise from nuclear quadrupolar effects alter the appearance of a frozen solution spectrum in much the way that Figures 4 and 5 differ.

Frozen solution spectra of the other anion radicals were analyzed by hand using eq 7, 8, and 9 and $\alpha = 15°$. The resulting parameters are also given in Table II.

Discussion

Electron-nuclear hyperfine interactions arise from classical dipole-dipole coupling as well as the isotropic Fermi contact interaction,[15] and the hyperfine tensor may be expressed as a

Table III. LUMO Orbital Percent Composition

molecule	$3d_{z^2}$	$3d_{yz}$	$3d_{x^2-y^2}$	4s	4p	α, deg
$RC_2R'Co_2(CO)_6$[a]	25–21	7–11	0.1–0.0	0.8		15–20
$H_4N_2Fe_2(CO)_6$[b]	16.5	7.5	0.0	0.0	5.3	24.0
$(CH_3)_2N_2Fe_2(CO)_6$[b]	20.0	6.2	0.5	0.4	6.4	21.5
$(CH_3)_2S_2Fe_2(CO)_6$[b]	23.6	3.3	0.0	0.1	6.0	19.0
$S_2Fe_2(CO)_6$[b]	24.6	2.8	0.6	0.1	6.7	15.2

[a] R = CF_3; R′ = $Si(CH_3)_3$. [b] Reference 9.

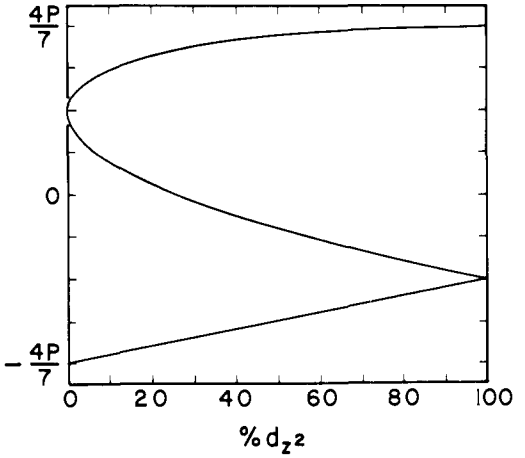

Figure 6. Dipolar hyperfine tensor components for d_{z^2}–d_{yz} admixtures.

sum of terms representing the two effects:

$$a_{ij} = b_{ij} + \langle a \rangle \delta_{ij} \tag{10}$$

Second-order contributions to eq 10, arising from spin–orbit coupling and proportional to $(g_{ij} - g_e)$, are often important for transition-metal complexes.[16] In the present case, however, the g-tensor components are close to the free-electron value and we will ignore spin–orbit contributions to eq 10. If a single 3d orbital on atom i contributes to the molecular orbital wave function, the dipolar contribution[17] to the hyperfine tensor for nucleus i is given by

$$b_i = |\mp 4/7 \pm 2/7 \pm 2/7| P\rho_i{}^{3d} \tag{11}$$

where $\rho_i{}^{3d}$ is the 3d-orbital spin density, and P is given by

$$P = g_e g_N \mu_B \mu_N \langle r^{-3} \rangle \tag{12}$$

The upper signs in eq 11 apply to d_{xy}, d_{xz}, d_{yz}, and $d_{x^2-y^2}$ while the lower signs apply when the electron is in a d_{z^2} orbital.

If the contribution of atomic orbitals on atom i to the molecular orbital containing the unpaired electron is described as a linear combination of the real 3d orbitals

$$c_1|z^2\rangle + c_2|yz\rangle + c_3|xz\rangle + c_4|x^2 - y^2\rangle + c_5|xy\rangle \tag{13}$$

then the hyperfine tensor is generally no longer diagonal in the xyz coordinate system. For the general case of eq 13, the dipolar tensor components are given by

$$b_{ij} = (2/7)P\rho^{3d} l_{ij} \tag{14}$$

where the l_{ij} are given by eq 15a–f.

$$l_{xx} = -c_1{}^2 - 2c_2{}^2 + c_3{}^2 + c_4{}^2 + c_5{}^2 - 2\sqrt{3}c_1c_4 \tag{15a}$$

$$l_{yy} = -c_1{}^2 + c_2{}^2 - 2c_3{}^2 + c_4{}^2 + c_5{}^2 + 2\sqrt{3}c_1c_4 \tag{15b}$$

$$l_{zz} = 2c_1{}^2 + c_2{}^2 + c_3{}^2 - 2c_4{}^2 - 2c_5{}^2 \tag{15c}$$

$$l_{xy} = -2\sqrt{3}c_1c_5 + 3c_2c_3 \tag{15d}$$

$$l_{xz} = \sqrt{3}c_1c_3 + 3c_3c_4 + 3c_2c_5 \tag{15e}$$

$$l_{yz} = \sqrt{3}c_1c_2 + 3c_3c_5 - 3c_2c_4 \tag{15f}$$

Thus, for example, for a combination of only d_{z^2} and d_{yz} orbitals, the hyperfine tensor given by eq 16 is obtained.

$$l = \begin{vmatrix} -c_1{}^2 - 2c_2{}^2 & 0 & 0 \\ 0 & -c_1{}^2 + c_2{}^2 & \sqrt{3}c_1c_2 \\ 0 & \sqrt{3}c_1c_2 & 2c_1{}^2 + c_2{}^2 \end{vmatrix} \tag{16}$$

This tensor may be diagonalized by rotation about the x axis by the angle α, given by

$$\alpha = (1/2) \tan^{-1} (2c_2/\sqrt{3}c_1) \tag{17}$$

to give the components shown in Figure 6. Here we see that the dipolar interaction tensor is not axial; indeed, binary combinations of d_{z^2} with any of the other d orbitals gives in general a completely anisotropic dipolar tensor. Similarly binary combinations of $d_{x^2-y^2}$ with d_{xz} or d_{yz} result in nonaxial tensors, but binary combinations of d_{xy} and $d_{x^2-y^2}$ or ternary combinations of d_{xy}, d_{xz}, and d_{yz} give axial tensors with components given by eq 11.

The parameter P, given by eq 12, can be computed from atomic orbital wave functions. A recent calculation by Morton and Preston[18] gives P = 6.71 MHz (30.2 mT) for ^{59}Co atoms. The value of P is expected to increase with net positive charge on the cobalt atom, probably by about 10% for each unit of charge.[5] In the present analysis, we shall use P = 30.2 mT but note that, because of the unknown charge on the cobalt atoms in $RC_2R'Co_2(CO)_6^{-\cdot}$ and the inherent error involved in using a value of P computed from atomic orbitals in a molecular orbital description, the resulting uncertainties are on the order of at least 10–20%.

The isotropic cobalt hyperfine coupling constant results from spin polarization of the filled 1s, 2s, and 3s orbitals as well as the filled molecular orbitals having a 4s contribution. The negative contribution to $\langle a \rangle$ from polarization of the 1s and 2s orbitals is expected to dominate. In addition, any 4s character in the molecular orbital containing the unpaired electron would make a positive contribution to $\langle a \rangle$. In the $YCCo_3(CO)_9$ anion radicals, the unpaired electron occupies an a_2 orbital which can contain no 4s character;[19] In this case the observed coupling, $\langle a \rangle \simeq -3.5$ mT, must arise entirely from polarization. From the anisotropic coupling, one can estimate $\rho^{3d} \simeq 0.25$. If we assume that the polarization contribution to $\langle a \rangle$ is proportional to ρ^{3d}, $a \simeq Q\rho^{3d}$, then $Q = -14$ mT. Morton and Preston[18] compute 212 mT for the isotropic coupling of a single cobalt 4s electron. The two contributions may then be combined:

$$\langle a \rangle = -14\rho^{3d} + 212\rho^{4s} \tag{18}$$

Thus, given $\langle a \rangle$ and ρ^{3d}, we can obtain a rough estimate of the 4s contribution to the molecular orbital.

Turning now to the $RC_2R'Co_2(CO)_6$ radical anions, we take the C–C vector to define the molecular x axis and the Co–Co vector to define the molecular z axis. We assume that these axes, and the perpendicular y axis (the C_2 axis under C_{2v} symmetry), are the principal axes of the g tensor. For the purposes of the following discussion,[20] we shall take the local axes on each cobalt atom to be parallel to the molecular axes

as defined. With this choice of axes, the d_{z^2}, d_{yz}, $d_{x^2-y^2}$, s, p_z, and p_y cobalt orbitals contribute to molecular orbitals of a_1 and b_2 symmetry whereas the d_{xz}, d_{xy}, and p_x orbitals contribute to a_2 and b_1 molecular orbitals.

Let us now examine the implications of the dipolar hyperfine tensor. For the $[CF_2C_2Si(CH_3)_3]Co_2(CO)_6$ radical anion, $\langle a \rangle = \mp 2.66$ mT and $b = |\mp 3.83\ \mp 1.54\ \pm 5.37|$ mT. Assuming that the metal contribution to the molecular orbital containing the unpaired electron (the lowest unoccupied MO of the neutral parent molecule which we shall hereafter refer to as the LUMO) is entirely 3d, we can immediately reject molecular orbitals of a_2 and b_1 symmetry since any combination of d_{xy} and d_{xz} would result in an axial hyperfine tensor.

When we consider the d-orbital combinations of a_1 or b_2 symmetry, three orbitals are found which give dipolar tensors which duplicate the experimental component ratios. Each of the three orbitals is essentially similar in shape to one of the component atomic orbitals—d_{z^2}, d_{yz}, or $d_{x^2-y^2}$—but the detailed description of each depends upon the orientation of its principal axes relative to the coordinate system in which the basis set is defined. The orientation-dependent composition of each orbital is shown in Figure 7. The dipolar tensors corresponding to the three orbitals are given by

$$\text{for "}d_{z^2}\text{": } b = |-0.396\ -0.159\ +\ 0.555|P\rho^{3d} \quad (19a)$$

$$\text{for "}d_{yz}\text{": } b = |+0.159\ -0.555\ +0.396|P\rho^{3d} \quad (19b)$$

$$\text{for "}d_{x^2-y^2}\text{": } b = |-0.555\ +0.396\ +\ 0.159P\rho^{3d} \quad (19c)$$

The first component in each case corresponds to the x axis while the second and third components correspond to principal axes in the yz plane. The experimental results provide a unique choice among these three possibilities. The experimental hyperfine tensor component, $b_1 = \mp 3.83$ mT, belongs to a principal axes common to both cobalt atoms, necessarily the x axis. This assignment can be made only for the orbital resembling d_{z^2}. *This assignment also determines the sign of the tensor components unambiguously.*

Comparison of the experimental and calculated dipolar hyperfine interaction tensors leads to $P\rho^{3d} = 9.68$ mT, which, with $P = 30.2$ mT, leads to $\rho^{3d} = 0.32$. Thus the total cobalt 3d character in the molecular orbital is about 64%. Furthermore, with this value of ρ^{3d} and $\langle a \rangle = -2.66$ mT, eq 18 gives $\rho^{4s} = 0.008$.

Consider now the angle α, which describes the orientation of the dipolar tensor principal axes in the yz plane. From the simulation studies described above, we found that α is 15–20°. There are then four possible orientations of the major principal axis, corresponding to $b_3 = +5.37$ mT, relative to the molecular z axis: $\pm\alpha$ and $\pm(90 - \alpha)$. As we expect the LUMO to be strongly antibonding, orientation at $\pm(90 - \alpha)$ is unlikely and we conclude that the major axes of the d_{z^2}-like orbital contributions to the LUMO are orientated at $\pm\alpha$ with respect to the Co-Co vector.

The cobalt 3d contributions to the LUMO, obtained from Figure 7a for $\alpha = 15$–20°, are given in Table III. Also given in Table III are the LUMO populations for several structurally related bridged $X_2Fe_2(CO)_6$ molecules obtained from molecular orbital theory calculations of Teo et al.[9] In every respect, the agreement between our experimental results for the $RC_2R'Co_2(CO)_6$ radical anions and the theoretical results for the bridged diiron molecules is striking.[22] However, by comparison with the molecular-orbital calculations, it appears likely that each cobalt also contributes ca. 6% 4p character to the LUMO. The contribution of 4p character to the dipolar hyperfine tensor has been ignored in our analysis, but, since $\langle r^{-3} \rangle_{4p}$ is considerably smaller than $\langle r^{-3} \rangle_{3d}$, this omission is probably not important. If we assume ca. 6% 4p, together with 32% 3d and 1% 4s character, we are left with about 22% total ligand orbital contribution to the LUMO. If the molecular orbital theory calculations are taken as a guide,[9] this contribution is spread more or less evenly among the six carbonyl ligands and the bridging acetylene moiety.

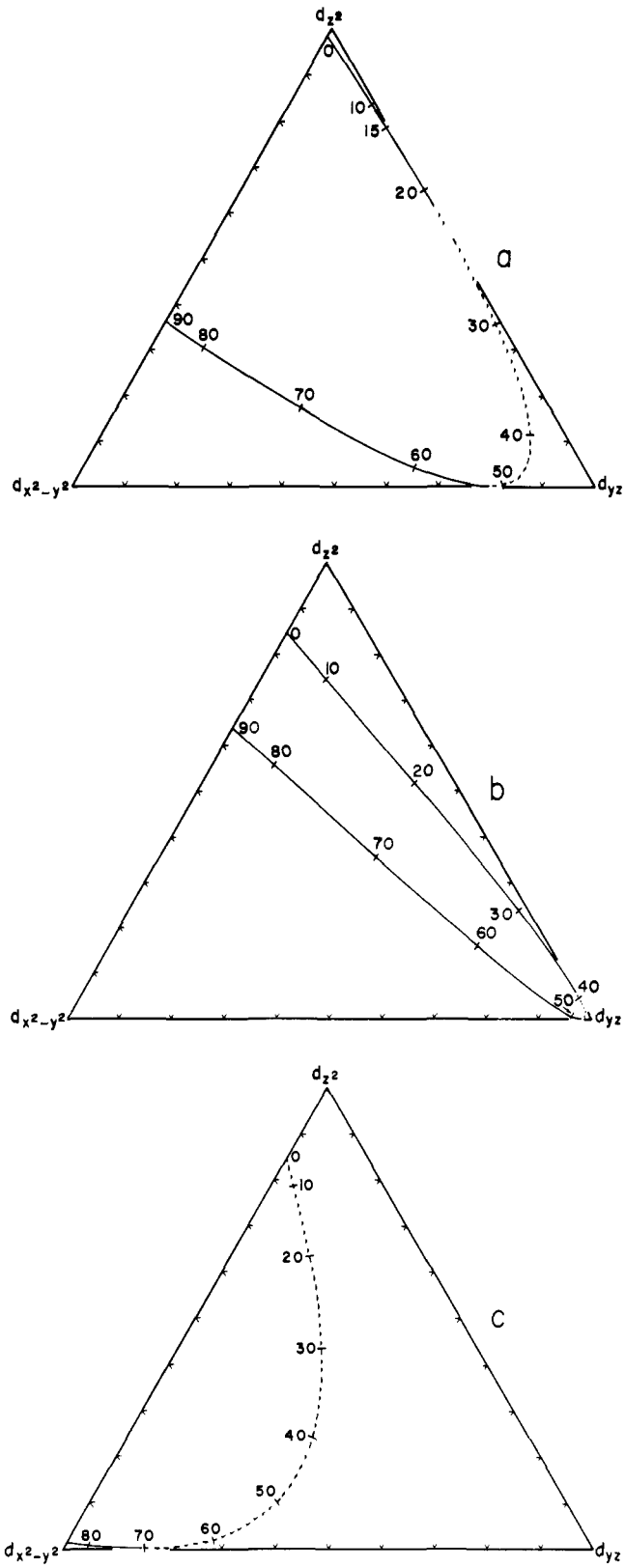

Figure 7. Molecular orbital compositions which fit the relative magnitudes of the experimental dipolar hyperfine tensor components. Dashed portions of the curves represent regions where the coefficients of d_{z^2} and $d_{x^2-y^2}$ are of opposite sign. The angle between the molecular z axis and the orbital major axis in indicated at various points on the curves.

Spin-orbit coupling of the b_2 orbital containing the unpaired electron

$$|b_2\rangle_0 = c_{10}[|z^2\rangle_1 - |z^2\rangle_2] + c_{20}[|yz\rangle_1 + |yz\rangle_2] + c_{40}[|x^2-y^2\rangle_1 - |x^2-y^2\rangle_2] + \ldots \quad (20)$$

with filled molecular orbitals of a_1, b_1, and a_2 symmetry

$$|a_1\rangle_l = c_{1l}[|z^2\rangle_1 + |z^2\rangle_2] + c_{2l}[|yz\rangle_1 - |yz\rangle_2] + c_{4l}[|x^2-y^2\rangle_1 + |x^2-y^2\rangle_2] + \ldots \quad (21a)$$

$$|b_1\rangle_m = c_{3m}[|xz\rangle_1 - |xz\rangle_2] + c_{5m}[|xy\rangle_1 + |xy\rangle_2] + \ldots \quad (21b)$$

$$|a_2\rangle_n = c_{3n}[|xz\rangle_1 + |xz\rangle_2] + c_{5n}[|xy\rangle_1 - |xy\rangle_2] + \ldots \quad (21c)$$

leads to deviations of the g-tensor components from the free-electron value. These may be computed, using the method of Stone,[23] to obtain

$$g_x - g_e = 8\xi\sum_l \frac{[\sqrt{3}c_{10} + c_{40})c_{2l} - c_{20}(\sqrt{3}c_{1l} + c_{4l})]^2}{E_0 - E_l} \quad (22a)$$

$$g_y - g_e = 8\xi\sum_m \frac{[(\sqrt{3}c_{10} - c_{40})c_{3m} + c_{20}c_{5m}]^2}{E_0 - E_m} \quad (22b)$$

$$g_z - g = 8\xi\sum_n \frac{[c_{20}c_{3n} - 2c_{40}c_{5n}]^2}{E_0 - E_n} \quad (22c)$$

where ξ is the spin-orbit parameter. According to the molecular orbital theory calculations by Teo et al.,[9] the b_2 LUMO is ca. 5 eV higher in energy than the a_1 HOMO, which is the principal metal-metal bonding orbital. However, these two orbitals have virtually the same 3d contributions so that $c_{i0} \simeq c_{il}$ and the numerator of eq 22 is nearly zero for that term. The remaining molecular orbitals having substantial metal 3d character lie 6-7 eV below $|b_2\rangle_0$; thus the differences among g_x, g_y, and g_z depend upon the details of the 3d orbital populations in the filled molecular orbitals in this energy range. However, we note that, taking $\xi \sim 100$ cm^{-1},[24] $8\xi/(E_0 - E_n)$ is on the order of 0.02, in agreement with the magnitude of the $g_i - g_e$ found experimentally.

According to the MO energy level scheme of Thorn and Hoffmann,[10] on the other hand, the b_2 LUMO lies about 4 eV above the HOMO which is of a_2 symmetry with significant acetylene π^* character; the a_1 metal-metal bonding orbital and a b_1 orbital lie ca. 0.5 eV lower in energy. With this scheme, g_y and g_z are expected to be greater than g_x as is observed. Furthermore, g_y and g_z should be sensitive to the nature of the acetylene substituents. Variations in g_y and g_z are comparable with experimental uncertainties, but it seems significant that the isotropic g value is greatest for the CF_3-substituted acetylenes, suggesting that the b_2-a_2 and/or b_2-b_1 energy differences are smaller. This is consistent with the observed lowering of polarographic reduction potentials for the CF_3-substituted acetylenes.[7]

It should be noted that the angle α, determined experimentally and therefore completely independent of any assumptions about the nature of the molecular orbital, describes the orientation of maximum electron density with respect to the Co-Co vector. To the extent that the orbital containing the unpaired electron is the antibonding counterpart of the principal metal-metal bonding orbital, α is the angle of the metal-metal bonding interaction with respect to the metal-metal vector. Thus the detailed agreement with the molecular orbital theory calculations on the X_2Fe_2 systems merely strengthens the conclusion that the metal-metal interaction in the $RC_2R'Co_2(CO)_6$ compounds can be accurately described in terms of a "bent" bond.

Although the above analysis has been in terms of the $[CF_3C_2Si(CH_3)_3]Co_2(CO)_6$ radical anion for which detailed spectrum simulations were obtained, examination of the results in Table II leaves no doubt that this description is appropriate for the other dicobalt acetylenes as well. The $P_2Co_2(CO)_6$ and $As_2Co_2(CO)_6$ radical anions[7] gave poorly resolved frozen solution spectra, but the similarities of the isotropic g values and cobalt coupling constants strongly suggest that these radicals are also very similar in electronic structure.

Note Added in Proof. A recent MO theory calculation by Fisel and Hoffmann (R. Hoffmann, private communication) on $H_2C_2Co_2(CO)_6$ gives a LUMO with a metal d-orbital mixture in good agreement with the results reported here but with substantially greater ligand orbital participation (ca. 47%). The calculation showed substantial mixing of metal 3d character with the numerous carbonyl π^* orbitals suggesting that the above discussion of the excited states and the g tensor is probably greatly oversimplified.

Acknowledgment is made to the donors of the Petroleum Research Fund, administered by the American Chemical Society, for partial support of this research. P.H.R. thanks the Department of Chemistry, University of Otago, for their hospitality during 1977-1978 when this work was begun.

Appendix

Analysis of the spectra reported in this paper was carried out using the spin Hamiltonian

$$\hat{H} = \mu_B \vec{B} \cdot \underline{g} \cdot \vec{S} + \sum_i \vec{S} \cdot \underline{A}_i \cdot \vec{I}_i \quad (A1)$$

where $\vec{B}$ is the magnetic field, $\vec{S}$ is the electron spin operator, $\vec{I}_i$ is the nuclear spin operator for the ith nucleus, and μ_B is the Bohr magneton. The g tensor, $\underline{g}$, and hyperfine tensors, $\underline{A}_i$, are assumed to share one principal axis; the remaining hyperfine tensor principal axes are displaced from the corresponding g-tensor axes by an angle α_i. Nuclear quadrupolar and nuclear Zeeman terms are assumed to be negligible. The Hamiltonian was solved by the methods of Blinder[25] to obtain eq A2 for the resonant magnetic field.

$$B = B_0 - \sum_i k_i m_i + \sum_i \left(\frac{m_i^2}{2g^2B_0}\right)\left(\frac{(g^2k_i^2 - g_1^2a_{i1}^2)(g^2k_i^2 - g_b^2b_i^2)}{g^2k_i^2} + \frac{(g^2k_i^2 - g_1^2a_{i1}^2)(g_b^2b_i^2 - g_2^2a_{i2}^2)(g_b^2b_i^2 - g_3^2a_{i3}^2)}{g^2k_i^2(g_b^2b_i^2 - g_1^2a_{i1}^2)}\right) - \sum_i \left(\frac{I_i(I_i+1) - m_i^2}{4g^2B_0}\right)\left(\frac{g_1^2a_{i1}^2g_b^2b_i^2}{g^2k_i^2} + \frac{g_2^2a_{i2}^2g_3^2a_{i3}^2}{g_b^2b_i^2} + \frac{g_1^2a_{i1}^2(g^2k_i^2 - g_b^2b_i^2)(g_b^2b_i^2 - g_2^2a_{i2}^2)(g_b^2b_i^2 - g_3^2a_{i3}^2)}{g^2k_i^2g_b^2b_i^2(g_b^2b_i^2 - g_1^2a_{i1}^2)}\right) \quad (A2)$$

The parameters of eq A2 are related to the components of the g and hyperfine tensors by eq A3-A10; the angles θ and ϕ describe the orientation of the magnetic field in the g-tensor principal axis coordinate system. Equation A2 reduces to the result given by Atherton and Winscom[11] when $\alpha_i = 0$ and to eq 2 when $\theta = 0$ or $\theta = 90°$, $\phi = 0$ or 90°.

$$B_0 = h\nu_0/\mu_B g \quad (A3)$$

$$a_i = A_i/g_i\mu_B \quad (A4)$$

$$g^2 = g_1^2 \cos^2\theta + g_b^2 \sin^2\theta \quad (A5)$$

$$g_b^2 = g_2^2 \cos^2\phi + g_3^2 \sin^2\phi \quad (A6)$$

$$k_i^2 = (g_1/g)^4 a_{i1}^2 \cos^2\theta + (g_b/g)^4 b_i^2 \sin^2\theta \quad (A7)$$

$$b_i^2 = (g_2/g_b)^2 a_{i2}^2 \cos^2(\phi' + \alpha_i) + (g_3/g_b)^2 a_{i3}^2 \sin^2(\phi' + \alpha_i) \quad (A8)$$

$$\cos\phi' = (g_2/g_b)\cos\phi \quad (A9)$$

$$\sin\phi' = (g_3/g_b)\sin\phi \quad (A10)$$

A Fortran program was written which computes the resonant field for each of 4096 orientations of the molecule using eq A2 and then constructs a histogram of the number of resonant conditions found in each of 1575 equal field increments spanning the range of the experimental spectrum. The component powder patterns are then added and artificially broadened by computing the convolution integral with the appropriate Gaussian or Lorentzian shape function. The result is then differentiated and plotted. The program is based on a general approach to magnetic resonance powder patterns developed by Taylor and Bray[26] but with provisions added for more than one nucleus and noncoincident tensor axes. Since for two spin $^7/_2$ nuclei there are 64 components, the program computes over 262 000 resonant field values for each spectrum and is therefore expensive to run, each spectrum requiring approximately 40 min on an IBM 370/138 computer.

References and Notes

(1) Part 8: P. Dawson, B. M. Peake, B. H. Robinson, and J. Simpson, *Inorg. Chem.*, in press.
(2) (a) University of Otago; (b) Brown University.
(3) R. E. Tapscott and R. L. Belford, *Inorg Chem.*, **6**, 735–743 (1967); T. D. Smith, J. F. Boas, and J. R. Pilbrow, *Aust. J. Chem.*, **27**, 2535–2545 (1974).
(4) P. D. W. Boyd, A. D. Toy, T. D. Smith, and J. R. Pilbrow, *J. Chem. Soc., Dalton Trans.* 1549–1563 (1973).
(5) A. J. Freeman and R. E. Watson, "Magnetism", Vol. IIA, G. T. Rado and H. Suhl, Eds., Academic Press, New York, 1965, pp 167–305.
(6) P. W. Atkins and M. C. R. Symons, "The Structure of Inorganic Radicals", Elsevier, Amsterdam, 1967.
(7) R. J. Dickson, B. M. Peake, P. H. Rieger, B. H. Robinson, and J. Simpson, *J. Organomet. Chem.*, **172**, C63 (1979).
(8) P. S. Braterman, *Struct. Bonding (Berlin)*, **10**, 57–86 (1972).
(9) B. K. Teo, M. B. Hall, R. F. Fenske, and L. F. Dahl, *Inorg. Chem.*, **14**, 3103–3117 (1975).
(10) D. L. Thorn and R. Hoffmann, *Inorg. Chem.*, **17**, 126–140 (1978).
(11) N. M. Atherton and C. J. Winscom, *Inorg. Chem.*, **12**, 383–390 (1973).
(12) P. W. Atkins and M. C. R. Symons, *J. Chem. Soc.*, 4363–4368 (1964); F. A. Cotton and E. Pedersen, *J. Am. Chem. Soc.*, **97**, 303–308 (1975).
(13) R. S. Dickson and P. J. Fraser, *Adv. Organomet. Chem.*, **12**, 323–377 (1974).
(14) R. L. Belford and D. C. Duan, *J. Magn. Reson.*, **29**, 293–307 (1978).
(15) N. M. Atherton, "Electron Spin Resonance", Ellis Horwood, Chichester, 1973, p 126.
(16) A. Abragam and M. H. L. Pryce, *Proc. R. Soc. London, Ser. A*, **205**, 135–153 (1951).
(17) Reference 15, p 242.
(18) J. R. Morton and K. F. Preston, *J. Magn. Reson.*, **30**, 577–582 (1978).
(19) B. M. Peake, B. H. Robinson, J. Simpson, and D. J. Watson, *Inorg. Chem.*, **16**, 405–410 (1977); B. M. Peake, P. H. Rieger, B. H. Robinson, and J. Simpson, to be published.
(20) Teo et al. use a local coordinate system in which the z axes on the metal atoms are oriented in the direction of the axial carbonyl ligands. In the case of the dicobalt acetylenes, this would result in local z axes oriented at 28° relative to the Co–Co axis.[21]
(21) F. A. Cotton, J. D. Jamerson, and B. R. Stults, *J. Am. Chem. Soc.*, **98**, 1774–1779 (1976).
(22) With a basis set defined in terms of the alternative local coordinate axes,[20] the molecular orbital containing the unpaired electron contains 3d contributions from each cobalt of 27–30% $3d_{z^2}$, 5–2% $3d_{yz}$, and 0.2–0.3% $3d_{x^2-y^2}$.
(23) A. J. Stone, *Proc. R. Soc. London, Ser. A*, **271**, 424–434 (1963).
(24) J. E. Wertz and J. R. Bolton, Electron Spin Resonance", McGraw-Hill, New York, 1972, p 277.
(25) S. M. Blinder, *J. Chem. Phys.*, **33**, 748–752 (1960).
(26) P. C. Taylor and P. J. Bray, *J. Magn. Reson.*, **2**, 305–331 (1970); P. C. Taylor, J. F. Baugher, and H. Kriz, *Chem. Rev*, **75**, 203–240 (1975).

The Methylmercury Heavy Atom Effect. Phosphorescence Polarization and Triplet Spin Sublevel Radiative Activities of the CH_3Hg^{II}–Benzimidazole and CH_3Hg^{II}–Tryptophan Complexes

R. R. Anderson and A. H. Maki*

Contribution from the Department of Chemistry, University of California, Davis, California 95616.

Received April 23, 1979

Abstract: The triplet-state kinetics of the complexes of benzimidazole (HBIm) and tryptophan (HTrp) with CH_3Hg^{II} have been investigated. The sublevel relative radiative rate constants and total decay rate constants are reported for both complexes. The heavy-atom effect causes the largest radiative enhancements of in-plane spin sublevels. Results of the sublevel total decay rate constant measurements confirm the previously reported reduction factor of 40 in the triplet state lifetime of the $CH_3HgHBIm^+$ complex. The triplet lifetime of CH_3HgTrp is reduced by a factor of 800 relative to that of HTrp. Polarized phosphorescence excitation measurements were made on both complexes. The CH_3HgTrp complex has a polarization of $P = -0.18$, constant over the ^1L_a and ^1L_b absorption bands indicating out-of-plane polarization, while $CH_3HgHBIm^+$ has $P = 0.06$ over the ^1L_a band and $P = -0.06$ over the ^1L_b band indicating in-plane polarization. A new transient microwave-phosphorescence measurement is described which permits the measurement of average triplet lifetimes in the presence of optically competing chromophores.

I. Introduction

The uptake of CH_3Hg^{II} in biological systems[1-3] has been an area of great interest in recent years. Since the neurotoxicity of CH_3Hg^{II} to humans has been convincingly demonstrated,[4,5] a major concern has been to identify the critical sites of action. Potential candidates for CH_3Hg^{II} binding sites have been suggested and include the bases of DNA and RNA, primary amines, and sulfhydryl groups.[6-15]

It has been demonstrated previously[16,17] that the attachment of heavy closed-shell metal ions to aromatic chromophores of biopolymers results in an external heavy-atom effect.[18] The triplet quantum yield is enhanced with a corresponding quenching of fluorescence and a shortening of the triplet radiative lifetime. Frequently, the phosphorescence quantum yield is enhanced.[19] Optically detected magnetic resonance (ODMR) slow passage[20,21] and transient[22-24] methods may

0002-7863/80/1502-0163$01.00/0